

1 Differentiating between crop and soil effects on soil moisture 2 dynamics

3 Helen Scholz¹, Gunnar Lischeid^{2,3}, Lars Ribbe¹, Ixchel Hernandez Ochoa⁴, Kathrin Grahmann²

4 ¹Institute for Technology and Resources Management in the Tropics and Subtropics (ITT), TH Köln, Cologne, Germany

5 ²Leibniz Centre for Agricultural Landscape Research (ZALF), Müncheberg, Germany

6 ³Institute for Environmental Sciences and Geography, University of Potsdam, Potsdam, Germany

7 ⁴Institute of Crop Science and Resource Conservation (INRES), Crop Science Group, University of Bonn, Bonn, Germany

8 *Correspondence to:* kathrin.grahmann@zalf.de

9 **Abstract.** There is urgent need to develop sustainable agricultural land use schemes. Intensive crop production has induced
10 increased greenhouse gas emissions and enhanced nutrient and pesticide leaching to groundwater and streams. Climate change
11 is also expected to increase drought risk as well as the frequency of extreme precipitation events in many regions.
12 Consequently, sustainable management schemes require sound knowledge of site-specific soil water processes that explicitly
13 take into account the interplay between soil heterogeneities and crops. In this study, we applied a principal component analysis
14 to a set of 64 soil moisture time series from a diversified cropping field featuring seven distinct crops and two weeding
15 management strategies.

16 Results showed that about 97% of the spatial and temporal variance of the data set was explained by the first five principal
17 components. Meteorological drivers accounted for 72.3% of the variance, 17.0% was attributed to different seasonal behaviour
18 of different crops. While the third (4.1%) and fourth (2.2%) principal component were interpreted as effects of soil texture and
19 cropping schemes on soil moisture variance, respectively, the effect of soil depth was represented by the fifth component
20 (1.7%). However, neither topography nor weed control had a significant effect on soil moisture variance. Contrary to common
21 expectations, soil and rooting pattern heterogeneity seemed not to play a major role. Findings of this study highly depend on
22 local conditions. However, we consider the presented approach generally applicable to a large range of site conditions.

23 **1 Introduction**

24 Agriculture plays a major role to ensure the provision of food to a growing global population. At the same time, climate change
25 is putting yield stability at risk due to extreme weather events, rising the need for sustainable management of resources, such
26 as water and soil (Trnka et al., 2014). The transformation from large homogeneously cropped fields towards diversified
27 agricultural landscapes has been identified as an opportunity that can contribute to climate adaptation due to the positive effects
28 on multiple ecosystem services (Tamburini et al., 2020), and cropping system resilience to climatic extremes (Birtal and
29 Hazrana, 2019). Additionally, crop diversification is highly beneficial by reducing soil erosion through permanent soil cover
30 (Paroda et al., 2015), and by improving resource use efficiency through wider crop rotations (Rodriguez et al., 2021).

31 In terms of soil water dynamics, crop and management diversification can lead to improved water-stable macro-aggregation,
32 reduced soil compaction and increased soil organic carbon, which can reduce soil water infiltration and improve water retention
33 (Alhameid et al., 2020; Fischer et al., 2014; Karlen et al., 2006; Koudahe et al., 2022; Nunes et al., 2018). Korres et al. (2015)
34 reported that spatial variability of soil moisture was mainly driven by soil characteristics, followed by crop cover and
35 management. Soil moisture is also affected by soil texture and pore size distribution (Krauss et al., 2010; Rossini et al., 2021;
36 Pan and Peters-Lidard, 2008). The quantification of the impact of these effects on soil moisture variability is important, for
37 instance for hydrological applications and adopted management practices in agriculture (Hupet and Vanclouster, 2002).
38 As the diversity of independent variables in agricultural systems increases, demands for frequency and spacing of soil moisture
39 measurements and related data interpretation grow. Therefore, soil sensor networks are receiving increased attention,
40 particularly in Precision Agriculture (PA; Bogen et al., 2022; Salam and Raza, 2020), where the main goal is to increase
41 efficiency and productivity at the farm level while minimizing the negative impacts on the environment (Taylor and Whelan,
42 2010). Soil sensor networks can meaningfully contribute to PA as they can be used for various purposes, including the
43 delineation of management zones (Khan et al., 2020; Salam and Raza, 2020). Still, one of the most important demands to be
44 fulfilled by soil sensor networks is soil moisture monitoring, as accurate measurement of soil water content can play an
45 important role in improving water management and therefore, crop yields (Salam, 2020).
46 Wireless solutions, for instance based on LoRaWAN (Long Range Wide Area Network) technology, in combination with
47 electromagnetic soil moisture sensors avoid labour-intensive and destructive soil moisture measurements that disrupt field
48 traffic. The development of such wireless sensor networks (WSN) enables broad and affordable application also in areas with
49 low cellular coverage (Cardell-Oliver et al., 2019; Lloret et al., 2021; Placidi et al., 2021; Prakosa et al., 2021).
50 The evolvement of WSN does not only have benefits for management but is also of high relevance for fostering the
51 understanding of hydrological dynamics in the vadose zone. High-resolution datasets measured under real farming conditions
52 can be used to characterize and analyse spatio-temporal dynamics of soil water. Due to the large size of data sets that are
53 recorded with WSN, sophisticated data analysis approaches are required to detect hidden patterns and determine influence
54 factors on soil moisture variability (Vereecken et al., 2014). With the introduction of multiple-points geostatistics, it became
55 possible to not only analyse patterns but also connect them with factors affecting soil moisture, such as topography, texture,
56 crop growth and water uptake, and land management (Brocca et al., 2010; Strebelle et al., 2003). Wavelet analysis can analyse
57 both localized features as well as spatial trends through which non-stationary variation of soil properties can be considered (Si,
58 2008). Cross-correlation analysis allowed linking soil moisture variability to climatic variables (Mahmood et al., 2012).
59 Furthermore, temporal stability analyses detect spots in the investigated area which are consistently wetter or drier than the
60 mean soil moisture (Baroni et al., 2013; Vachaud et al., 1985; Vanderlinden et al., 2012). This method was already successfully
61 used to detect soil moisture patterns related to soil properties, vegetation, and topography (Zhao et al., 2010).
62 Principal component analysis (PCA) is another method that was successfully applied for soil moisture variability analysis at
63 the field (Hohenbrink et al., 2016; Hohenbrink and Lischeid, 2015; Martini et al., 2017), catchment (Korres et al., 2010;
64 Lischeid et al., 2017; Nied et al., 2013; Graf et al., 2014), and regional (Joshi and Mohanty, 2010) scale. These studies build

65 on previous applications in climatology where the term “Empirical Orthogonal Functions” is used (Bretherton et al., 1992) and
66 are examples for how space and time dimensions can be disentangled and assigned to influencing factors. Additionally, the
67 propagation of hydrological signals (e.g. precipitation events) over depth can be assessed (Hohenbrink et al., 2016). This opens
68 up great opportunities to improve the knowledge of changing soil water dynamics in complex diversified agricultural systems
69 with increasing heterogeneity (e. g. soil texture) and site-specific adjustment of crop and field management which, to our
70 knowledge, have hardly been studied so far. The main objective of this study was to identify the drivers of soil moisture
71 variability in a diversified cropping field in terms of soil texture, crop selection and field management by applying PCA.
72 Special focus was put on the interpretation of spatial and temporal effects of crop diversification and of soil heterogeneities on
73 soil moisture dynamics. For this, we analysed a high-resolution soil moisture data set measured by a novel underground
74 LoRaWAN monitoring system with soil moisture sensors in different depths of the vadose zone at a spatial-temporally
75 diversified agricultural field in Northeast Germany. The novelty of this WSN relies on its unique on-farm installation
76 environment. The deployment of transmission units in 0.3 m soil depth and 180 sensors in up to 0.9 m soil depth allows high
77 spatio-temporal resolution wireless data transmission, and enables conventional farming practices like machinery traffic,
78 tillage and mechanical weeding.

79 **2 Materials and methods**

80 **2.1 Study site**

81 The study site (52°26'51.8"N 14°08'37.7"E, 66-83 m.a.s.l.) is located near the city of Müncheberg in the federal state of
82 Brandenburg in Northeastern Germany. The landscape is classified as a hummocky ground moraine that formed during the
83 last glacial periods. Glacial and interglacial processes as well as subsequent erosion resulted in highly heterogeneous soils
84 (Deumlich et al., 2018), being classified as Dystric Podzoluvisols according to the FAO scheme (Fischer et al., 2008). In the
85 top 0.3 m soil layer, total organic carbon was 0.94% and total nitrogen content was 0.07%, and pH was 6.12. Between January
86 1991 and December 2020, the mean annual temperature in Müncheberg was 9.6°C, and the mean annual sum of precipitation
87 was 509 mm (DWD Climate Data Center (CDC), 2021).

88 **2.2 Experimental setup**

89 The data collection was carried out from December 2020 until mid of August 2021 in the patchCROP experiment (Grahmann
90 et al, 2021; Donat et al., 2022). This landscape experiment has been set up to study the multiple effects of cropping system
91 diversification on productivity, crop health, soil quality, and biodiversity. To that end, a cluster analysis was carried out based
92 on soil maps and multi-year (2010 to 2019) yield data to identify high and low yield potential zones in the 70-ha large field
93 (Donat et al., 2022). Afterwards, single experimental units comprising 30 patches with an individual size of 0.52 ha (72 m ×
94 72 m) each, have been implemented in both, high and low yield potential zones where each of those zones is characterized by
95 varying soil conditions and a site-specific five-year, legume-based crop rotation (Grahmann et al., 2021). The remaining area

96 outside of the 30 patches was planted with winter rye. For the current study, twelve out of 30 patches were considered (Table
97 1, Figure 1). Specific patches were selected to capture the soil heterogeneities in terms of soil texture, but also the seasonal
98 patterns of the crop rotation that may have important effects on the soil water dynamics such as crop types, presence of cover
99 crops or fallow periods. In the cropping season 2020/2021, seven different main crops were grown. For subsequent data
100 interpretation, crops have been grouped into A) winter crops, B) fallow, followed by summer crops and C) cover crops,
101 followed by summer crops. In seven out of twelve considered patches, weed control was carried out with herbicide application,
102 referred as “conventional” pesticide application, while in the remaining five patches, “reduced” pesticide management was
103 carried out by mainly using mechanical weeding, by harrowing, blind harrowing, and hoeing. Only in the case of high weed
104 pressure herbicides were applied. Due to the potential impact of mechanical weeding, i.e., on rainwater infiltration, soil
105 evaporation and topsoil rooting intensity, we differentiate between these modes of weed control.

106 **2.3 Data collection**

107 **2.3.1 Soil moisture data**

108 Soil moisture was recorded by a long-range-wide-area network (LoRaWAN) based WSN. In each patch, one Dribox box
109 equipped with a SDI-12 distributor (serial data interface at 1200 baud rate, TBS04, TekBox, Saigon, Vietnam) connected to
110 six TDR-sensors (TDR310H, Acclima, Meridian, USA) and attached to an outdoor remote terminal unit (RTU) fully
111 LoRaWAN compliant (TBS12B: 4+1 channel analogue to SDI-12 interface for 24 Bit A/D conversion of sensor signals,
112 TekBox, Saigon, Vietnam) was installed as LoRa node. It was deployed at least 0.3 m below ground to allow field traffic and
113 soil tillage. The sensors and boxes were installed between August and November 2020. At two georeferenced locations within
114 each patch, soil moisture sensors were installed in 0.3, 0.6 and 0.9 m depth, respectively. Sensors were approximately 2 m
115 apart from the LoRa node in angles between 45° and 60° (Figure 1). Soil moisture sensors at 0.3 m were placed horizontally,
116 while sensors at 0.6 and 0.9 m depth were placed vertically using auger-made boreholes and extension tubes for soil insertion.
117 Communication of LoRa nodes was wireless and autarkic in energy supply. Thus, no electric cabling except from connections
118 between sensors and LoRa nodes was needed. Under optimum conditions, battery running time of the LoRa nodes can be up
119 to 12 months but can be reduced to 8 months when radio transmission is attenuated (e.g. due to near water-saturated soil)
120 which then increases power consumption (Bogena et al., 2009). Data was recorded every 20 minutes by the LoRa nodes
121 through a LoRa-WAN Gateway DLOS8 (UP GmbH, Ibbenbüren, Germany) which was equipped with the modem TL-
122 WA7510N (TP Link, Hong Kong, China) to transfer the data to a cloud from where collected data could be accessed directly
123 after the measurement. The time series included in this study covered the period from December 01, 2020, until August 14,
124 2021 (Figure 2).

125 **2.3.2 Weather data**

126 Precipitation and temperature data (Figure 3) with a 15 min temporal resolution were obtained from two weather stations
127 located in the Eastern and Western end of the main patchCROP field. Climatic water balance was calculated from precipitation
128 and potential evapotranspiration, both measured at the climate station by the German Weather Service in Müncheberg (DWD
129 Climate Data Center (CDC), 2021). This station was chosen due to its proximity to the study site.

130 **2.3.3 Remote senses data for vegetation dynamics**

131 Furthermore, drone imagery from May 20, 2021, May 31, 2021, and July 06, 2021, was used for vegetation assessment. The
132 drone fixed-wing UAV-based RS eBee platform (SenseFly Ltd., Cheseaux-Lausanne, Switzerland) was operated at noon time
133 and recorded multispectral imagery with a Parrot Sequoia+ camera (green, red, NIR, and red edge bands, spatial resolution of
134 0.105 m) and thermal imagery of the surface (only on May 31, 2021) with a senseFly Duet T camera with a spatial resolution
135 of 0.091 m (Table 2). The multispectral imagery was processed with Pix4D to obtain the Normalized Difference Vegetation
136 Index (NDVI), following Eq. (1):

$$137 \quad NDVI = \frac{NIR-Red}{NIR+Red} \quad (1)$$

138 in which NIR is the intensity of reflected near-infrared light (reflected by vegetation) and Red the intensity of reflected red
139 light (absorbed by vegetation). A digital elevation model with a spatial resolution of 1 m (GeoBasis-DE and LGB, 2021) was
140 used to calculate the slope (ArcGIS 10.7.0; ESRI, 2011) (Table 2).

141 **2.3.4 Soil information**

142 *Soil texture by layer*

143 Manual classification of soil texture by layer was carried out by collecting 140 samples in eight of twelve analysed patches.
144 Samples were taken with a 1 m-length Pürckhauer soil auger. Soil textural class was manually determined at the field by
145 applying the protocol “Finger test to determine soil texture according to DIN 19682-2 and KA5” (Sponagel et al., 2005).
146 Additionally, representative soil samples were collected and analysed at the laboratory to determine particle size distribution
147 for sand, silt, and clay (soil texture based on the German particle classification). Soil texture was analysed following the DIN
148 ISO 11277 (2002) reference method by wet sieving and sedimentation, using the SEDIMAT 4-12 (Umwelt-Geräte-Technik
149 GmbH, Germany). The sand fraction in this method is defined between 2 and 0.063 mm, according to IUSS Working Group
150 WRB (2015).

151 To extrapolate the laboratory-based soil particle distribution to the soil textural classes manually determined at the field the
152 high and low yield potential laboratory samples were pooled separately. The average soil particle distribution was calculated
153 for each soil textural class and assigned to the respective soil layer with that specific soil textural class. The soil texture analysis
154 showed that soil texture variability increased with depth. In the third layer (average bottom depth = 0.92 m), the sand and clay

155 content across 133 sampling points varied between 53% to 94% and 2% to 22%, respectively. Soil sampling points were
156 located 0.8 m and 2.5 m away from the soil moisture sensors to minimize damage risk.

157 *Topsoil proximally sensed data*

158 In October 2019, the “Geophilus” soil scanner system (Lueck and Ruehlmann, 2013) was used in the entire field to map soil
159 electrical resistivity (ERa) as a proxy for texture for the top soil, using reference soil samples to calibrate the readings. A total
160 of four georeferenced reference soil samples were taken until 0.25 m soil depth, and locations were selected based on the
161 proximal soil sensor data (sensor-guided sampling; Bönecke et al., 2021). The “Geophilus” system is based on sensor fusion
162 in which ERa sensors are coupled with a gamma-ray detector. Apparent electrical conductivity was measured by pulling one
163 or more sensor pairs mounted on wheels across the field where each pair of sensors measured a different soil depth. Amplitude
164 and phase were measured simultaneously using frequencies from 1 MHz to 1 kHz. Reference soil samples were analysed via
165 soil-particle size analysis according to DIN ISO 11277 (2002) and served as calibration information in order to estimate sand,
166 silt and clay content in the top 0.25 m soil for the entire field. A non-linear regression model was applied. The RMSE of sand
167 content (5.7%) was considerably smaller than the standard deviation of the sand content in the first layer from the manual soil
168 texture analysis (11.9%), indicating a satisfactory prediction performance. The gamma-sensor was used to minimize
169 uncertainties, being less sensitive to soil moisture than the ERa readings (Bönecke et al., 2021). The estimated sand content in
170 the upper 0.25 m at the study site varied between 69.1% and 81.2% and averaged 79.0% (Table 1, Figure 1).

171 **2.4 Data processing**

172 Soil moisture data were available at 20-minute intervals. Transmission failures due to discharged batteries, signal disturbances
173 after rainfall, in patches with a high density of biomass (e.g. maize), and theft of parts of the WSN led to data gaps that affected
174 in some cases all sensors of the WSN and amounted to 81 out of 257 days of the measuring period. The affected days were
175 therefore skipped for the analysis. Whereas time series of eight sensors were excluded due to a higher frequency of transmission
176 failures, in total, 64 time series were used for the analysis, and additional data gaps for single sensors were interpolated linearly.
177 Of all 20,668 interpolated gaps, 96% were shorter than two hours, 3% between two and six hours and 1% longer than six hours.
178 In 26 cases, gaps exceeded the duration of one day. The interpolation was justified as the differences between the values before
179 and after the gaps were within the measuring accuracy of 1 vol-% of the soil moisture sensors (Acclima Inc., 2019). As
180 indicated by the retailer, sensors might suddenly jump to a soil moisture value of 28.6% and go back to normal again after one
181 or few time steps. Thus, a data deletion procedure of abrupt jumps to 28.6 was created. To ensure equal weighting for the
182 subsequent analysis, all soil moisture time series were z-transformed to unit variance and zero mean each (cf. Hohenbrink and
183 Lischeid, 2015). As a consequence, differences of absolute values were not considered by the further analysis.

184 **2.4 Statistical analysis**

185 To identify common temporal patterns among single time series, the soil moisture data set was analysed by a principal
186 component analysis (PCA). In a first step, PCA decomposes the total variance of a multivariate data set into independent
187 fractions called principal components (PCs). The number of PCs is the same as the number of time series in the input data set.
188 Each PC consists of eigenvectors (loadings), scores, and eigenvalues. The scores reflect the temporal dynamics. The
189 importance of single principal components for single sites is represented by the loadings of each PC (Jolliffe, 2002; Lehr and
190 Lischeid, 2020). Loadings are the Pearson correlation coefficients of the single time series of the input data set with the scores
191 of each PC, respectively. The eigenvalues of the single PC are proportional to the variance that they explain. The PCs are
192 sorted in descending order of eigenvalues. Eigenvalues greater than one indicate that a PC explains more variance than a single
193 input time series could contribute to the total variance of the entire input data set (Kaiser, 1960). More details on principal
194 component analysis for time series analysis are found in Jolliffe (2002). The PCA was performed using the *prcomp* function in
195 R version 4.1.0 (R Development Core Team, 2021).

196 The scores of the principal components constitute time series. Every observed soil moisture z-transformed time series can be
197 presented at arbitrary precision as a combination of various principal components. When the data set consists of time series of
198 the same observable measured at different locations, the first principal component describes the mean behaviour inherent in
199 the data set. Subsequent principal components reflect typical modifications of that mean behaviour at single locations due to
200 different effects. Thus, generating synthetic time series as linear combinations of the first PC and another additional PC helps
201 to assign this additional PC to a specific effect. To that end, scores of that component have either been added to or subtracted
202 from those of the first component using arbitrarily selected factors. The two resulting graphs show how the respective PC
203 causes deviations from the mean behaviour of the data set.

204 The relations to soil and vegetation parameters were tested by computing the Pearson correlation coefficients between the
205 scores and arithmetic mean values of all input time series as well as the Pearson correlation coefficients between loadings and
206 sand content until 0.25 m depth, sensor depth, antecedent z-transformed soil moisture, slope, and drone imagery products
207 (NDVI and surface temperature). Eventually, the Wilcoxon-Mann-Whitney test was applied to check whether loadings can be
208 grouped by management parameters (crops, cover crops, weeding management). All statistical analyses were conducted with
209 R version 4.1.0 (R Development Core Team, 2021).

210 **3 Results**

211 **3.1 Manual soil texture analysis**

212 The transferability of texture information from the sampling point to the soil moisture sensor location was not ensured due to
213 high nugget effects. Furthermore, manual soil texture analysis data were not available for all analysed patches. Consequently,
214 they were not included into further analysis.

215 **3.2 Principal component analysis**

216 The principal component analysis yielded five components with Eigenvalues exceeding one, which accounted for >97% of the
217 total variance of the data set (Table 3).

218 **3.2.1 First principal component**

219 The first principal component explained 72.3% spatiotemporal variance of the data set. All loadings on the first PC were
220 negative (Appendix A). The Pearson correlation coefficient of the scores of the first principal component with the mean values
221 of all input time series was less than - 0.999 ($p < 0.01$), the correlation between the scores and the cumulative climatic water
222 balance ($P - ET_p$) was -0.969 ($p < 0.01$). Thus, the time series of the negative scores of this component represented the mean
223 behaviour of soil moisture driven by external factors such as precipitation, temperature, and seasons in general which affected
224 time series in the same way, although to different degrees (cf., Hohenbrink et al., 2016; Lischeid et al., 2021).

225 **3.2.2 Second principal component**

226 The second principal component explained 17.0% of the total variance. The loadings ranged from -0.801 to 0.760 with a
227 median of -0.030 (Figure 4). The loadings showed a crop group specific pattern. All winter crops (barley, oats, rye) had positive
228 loadings with only one exception in 0.9 m depth. The summer crops maize, soy, and sunflower exhibited negative loadings. In
229 contrast, the summer crop lupine exhibited mostly positive loadings, similar to the winter crops, although of slightly smaller
230 magnitude. According to the Wilcoxon-Mann test, the group of barley, oats, rye, and lupine differed significantly from the
231 group of maize, soy, and sunflower.

232 As described in the Methods section, synthetic time series were generated as a linear combination of PC1 and PC2 (Figure 5).
233 The graph resulting from applying a positive factor for PC2 represents a typical deviation from mean behaviour for sites that
234 exhibit positive loadings, e.g., winter crops (blue line). The opposite holds for the summer crops which load negatively with
235 PC2 (orange line). Both lines plot very close to each other in February and March. In contrast, the orange line shows lower
236 values than the blue line in December and January, indicating lower soil moisture at the summer crop patches. The inverse
237 holds for the subsequent summer period starting in early June, pointing to earlier and more rapid water uptake of the winter
238 crops. In July and August, the approximately constant level of the blue curve indicates that only summer crops continue to
239 consume water while winter crops are in their ripening phase and eventually harvested.

240 Lupine and sunflower were the summer crops which were sown first (March 30, 2021, and April 2, 2021, respectively). Maize
241 was sown on April 16, 2021, and soy on May 15, 2021. The loadings of lupine, which were rather performing like winter crops
242 than summer crops, indicated that lupine showed an early onset of intensive evapotranspiration, compared to other summer
243 crops, especially sunflower which was sown at the same time.

244 For further investigation of the vegetation effect on PCs, drone imagery taken at the end of May, when sowing has been
245 completed in all patches, and imagery taken at the beginning of July, when winter crops are in the ripening phase, was analysed.
246 The second PC's loadings of the time series from different sensors were compared to the Normalized Difference Vegetation

247 Index (NDVI; available for three dates) and surface temperature (only available for May 31, 2021) of the respective sensor
248 location as a proxy for actual evapotranspiration. At the end of May, the NDVI, as a proxy for photosynthesis potential, was
249 positively correlated with the loadings (Table 4). Surface temperature exhibited a negative correlation. The spatial pattern of
250 surface temperature is assumed to be inversely related to that of actual evapotranspiration. Thus, both proxies, NDVI and
251 surface temperature, support the inference that in this study positive loadings on this principal component represent sites with
252 above-average plant activity and root water uptake at the end of May. This holds for sensors from all depths but was the closest
253 for 0.9 m depth (Pearson correlation of $r = -0.916$ for surface temperature and of $r = 0.946$ for NDVI on May 31). The results
254 in July compared to those in May support the observation. At the time when the winter crops are already in the ripening phase
255 and the summer crops reach high levels of evapotranspiration, the correlations are being reversed and negative loadings
256 indicate above-average plant activity for summer crops. On July 06, highest Pearson correlations for NDVI are found for 0.6
257 m depth ($r = -0.917$).

258 **3.2.3 Third principal component**

259 The third PC explained 4.1% of the total data set's variance. Loadings ranged between -0.787 and 0.244 with a median of
260 0.006. Extreme loadings (<-0.25) were found only for sensors in 0.9 m depth in patches 66, 89, 95 and 102 (Figure 6). The
261 location of these patches shows a certain regional pattern, with the patches roughly following an east-west direction rather than
262 showing a random location within the field. This may point to topography or soil structure causing deviations from mean soil
263 moisture behaviour for patches located near this gradient. However, this pattern cannot be assigned to topography or structures
264 apparent on the topsoil map (Figure 1). Loadings were closely related to the minima of the z-transformed soil moisture in the
265 period from December to February ($r = 0.70$, $p < 0.001$, Figure 7). What distinguishes the orange line (negative loading on
266 PC3) from the blue line (positive loading on PC3) is the higher temporal variability and the delayed reaching of maxima in
267 the first half of the study period (Figure 8).

268 **3.2.4 Fourth principal component**

269 The fourth PC explained 2.2% of the total data set's variance. The loadings were clustered by crop groups. All fallow patches
270 showed consistent positive loadings while the patches which were covered by winter crops, showed mainly negative loadings
271 except in patch 95 where the loadings of the two sensors in 0.3 m depth were slightly above zero (Figure 9). According to the
272 Wilcoxon-Mann test treatment group B (fallow, followed by summer crops) differed significantly from group A (winter crops)
273 and C (cover crops, followed by summer crops) whereas there was no significant difference between group A and C. In contrast
274 to crop groups A and B, patches that were covered by the cover crop phacelia during the winter months, did not show one-
275 directional loadings.

276 Figure 10 illustrates the effect of the fourth PC on time series. The blue line (positive loading) shows a hydrological behaviour
277 which would be typical for more sandy soils while the orange line (negative loading) depicts behaviour that one would expect
278 in more loamy soils due to its delayed responses to rainstorms and subsequent less steep recovery. The patterns in the loadings

279 thus show a differentiation between patches with winter crops and fallow patches in the winter months (Figure 9). However,
280 it is not clear how winter crops on the one side and fallow on the other side could induce such a different soil water behaviour
281 shown in Figure 10.

282 **3.2.5 Fifth principal component**

283 The fifth PC explained 1.7% of the data set's variance. The loadings showed a depth-related pattern. All time series from the
284 0.3 m depth exhibited negative loadings with two minor exceptions. Whereas all time series from 0.9 m depth showed positive
285 loadings throughout, and time series from 0.6 m depth plot in between. Loadings in 0.6 m depth and 0.9 m depth were mostly
286 more similar to each other than to the loadings of 0.3 m depth (Figure 11). The Pearson correlation coefficient between loadings
287 and depth was $r = 0.710$ ($p < 0.05$). Thus it can be concluded that the fifth PC reflected the effect of soil depth on soil moisture
288 variance. This effect differed between crops, with the three most negative loadings found in maize patches while the three
289 most positive loadings were found in lupine patches. The soil water dynamics show a damping effect with increasing depth
290 (Figure 12) from little damping for sensors in the upper depth (orange line) to higher damping for sensors in greater depth
291 (blue line).

292 Neither patterns in topography nor in weeding management modes were reflected in the loadings of PC1-PC5. Due to the lack
293 of subsurface soil data, no additional findings could be derived from the Geophilus texture analysis.

294 **4 Discussion**

295 A PCA was conducted to identify the drivers of soil moisture variability in a diversified cropping field. Data consisted of
296 observed time series from 64 soil moisture probes. Results showed that the first five principal components described about
297 97% of the variance of the data set, and revealed various effects of weather, soil texture, soil depth, crops and management
298 schemes (Table 3). The first principal component captured 72% of the total variance. Consequently, 72% of the observed
299 dynamics could be described by a lumped model that would not consider any within-field heterogeneity. These results are in
300 the range of similar studies. Martini et al. (2017) found that the first PC explained 58% of the variance of a data set that
301 comprised both agricultural fields as well as grassland transects. Similarly, Lischeid et al. (2017) ascribed 70% of the variance
302 of a forest soil moisture data set to a single component. In the study by Hohenbrink et al. (2016), 85% of the variance of soil
303 moisture data in a set of arable field experiments with two different crop rotation schemes was attributed to the first principal
304 component. The strong influence of weather conditions as it is shown in our study is confirmed by Choi et al. (2007) who
305 showed that rainfall, next to topography, explained most of the surface soil moisture variability.

306 **4.1 Crop effects**

307 As Korres et al. (2015) stated that vegetation and management (e.g. planting and harvesting dates) are among the main causes
308 for spatial variability of soil moisture in agricultural fields. In this study, around 17% of the total variance at the field scale

309 was attributed to the vegetation effect. When not considering the temporal component reflected by PC1 and thus only looking
310 at the spatial variability, 61% of the remaining variance is caused by the vegetation effect reflected by PC2. Korres et al. (2010)
311 also used PCA to identify the drivers of spatial variability of soil moisture within a cropped area but did not find such a
312 pronounced vegetation effect. In their study, more than two thirds of the spatial variability was related to soil parameters and
313 topography. In contrast, the strong influence of vegetation in our study may be due to the high level of crop diversification.
314 Within single crop fields, vegetation effects are observable due to heterogeneous biomass or root development (Brown et al.,
315 2021; Korres et al., 2010), but may be of a lower magnitude compared to fragmented field arrangements with different crops.
316 The high impact of crop diversification on soil moisture variability is also visible when comparing our results to the results of
317 a field under comparable conditions in the same region with only two crop rotations in which only 3.8% was explained by the
318 different crop rotations (Hohenbrink et al., 2016). Joshi and Mohanty (2010) investigated spatial soil moisture variability at
319 the field to regional scale in the Southern Great Plains regions in the US by means of PCA and assessed the effect of vegetation
320 - in contrast to this study - as limited since none of the first seven PC showed strong correlations with vegetation parameters.
321 It needs to be considered that the proportion of the vegetation effect on soil moisture variability does not only vary spatially
322 and over depth, but also over time. Under dry conditions, soil-plant interactions prevail while under moist conditions,
323 percolation behaviour is predominant (Baroni et al., 2013). The scores are time series and reflect the effect size of a particular
324 process represented by the respective PC. The more the scores of a certain PC deviate from zero during specific periods, the
325 stronger the respective effect is. Consequently, the time series of PC2 scores indicates that the effect of vegetation on total
326 variability varies by time. In accordance with literature, the absolute values of the scores of PC2, representing differences
327 between the contrasting seasonality of crops, are highest in the dry months, May to August. This is mostly explained by the
328 high water demand of summer crops, which are in their vegetative growth stage from May to August, whereas winter crops
329 are already in their reproductive growth stage, including maturity, senescence and harvest where water uptake by crops is
330 minimal or absent (Zhao et al, 2018). In the moist winter months January to March, as well as during the heavy rainfall event
331 in July, the scores of PC2 are relatively small, showing that spatial variability at that time is caused by other factors.
332 The second principal component clearly differentiated between winter and summer crops, which was driven by the different
333 seasonal patterns of root water uptake (Figure 4). In contrast, the fourth component differentiated between fallow followed by
334 summer crops and winter crops, whereas phacelia followed by summer crop did not show a clear pattern (Figure 9). Phacelia
335 is grown as a cover crop and usually dies off in frost periods. Due to rather mild winter temperatures 2020/21, Phacelia was
336 not terminated efficiently and kept growing until spring, until it was terminated mechanically. It was recently shown that the
337 timing of removal of winter cover crops is key to provide soil water recharge for the subsequent crop, as the depletion of soil
338 water in autumn is significant (Selzer and Schubert, 2023). Thus, some Phacelia patches exhibited negative loadings, similarly
339 to the winter crop patches while other patches with most likely different termination dates exhibited positive loadings.
340 Hence, the fourth component obviously reflected the effect of the active root system in the winter period. According to this
341 component, soil water dynamics in the fallow patches mostly resembled the typical behaviour expected for sandy soils, and
342 winter crop patches showed a more damped behaviour that is usually observed in more loamy soils. Note that the term “fallow”

343 refers to crop cover in autumn and winter only. Acharya et al. (2019) found that winter cover crops improved soil moisture
344 from 3 to 5% in the top 0.3 m soil layer which is in line with the findings from Figure 10 that shows a higher water holding
345 capacity for winter crops (orange line) in winter. However, it has also been observed that roots from winter crops can increase
346 soil porosity and therefore, water mobility in the soil (Lange et al., 2013; Scholl et al., 2014).
347 Further soil-vegetation interactions might play a role for the delayed seepage fluxes of winter crop and part of cover crop
348 patches, such as soil organic matter from cover crops and plant residues (Manns et al., 2014; Rossini et al., 2021). Usually,
349 such effects are assumed to occur only at larger time scales, which is closely related to problems of detecting changes soil
350 organic carbon (SOC) quantity or quality. So far, there is only anecdotal evidence for rather short-term SOC quality affecting
351 soil hydraulic properties even at smaller time scales. Although this effect constituted only a minor share of soil moisture
352 variance (Table 3), it was clearly discernible as a separate principal component. This effect would be worth to be tested in
353 more detailed future studies.

354 **4.2 Soil texture and soil depth effects**

355 Loadings on the third principal component were not related to crop types. In contrast, a spatial pattern emerged: Only sensors
356 from 0.9 m depth from six adjacent patches exhibited strongly negative loadings (Figure 6), whereas all other sensors showed
357 minor positive or negative loadings. This points to an effect of subsoil substrates, that is, higher clay content and consequently
358 higher water holding capacity. That would be consistent with delayed response to seepage fluxes and reduced desiccation in
359 the vegetation period (Figure 8). The strong relation between z-transformed soil moisture minima at the beginning of the study
360 period (Figure 7) which might originate from a delayed response to a prior rainfall, and the regional pattern of the location of
361 the patches following a west-east direction within the experiment might be an indicator of underlying soil structures causing
362 this effect. Data on texture at soil moisture sensor locations in deeper layers would be of high value to confirm the assumptions.
363 Whereas the third principal component seems to reflect a local peculiarity, the fifth component obviously grasps a more generic
364 feature. Loadings on this component are clearly related with depth (Figure 11). Strong positive loadings indicate a strongly
365 damped behaviour of soil moisture time series: The blue line, representing sites with positive loadings on PC5 which is typical
366 for sensors at greater depth (Figure 12), exhibits clearly reduced amplitudes compared to the orange line, that is, sensors at
367 shallow depth. Hohenbrink and Lischeid (2015) combined a hydrological model and principal component analysis to study the
368 effect of soil depth and soil texture on damping of the input signal in more detail. A subsequent field study proved the relevance
369 of that effect in a real-world setting (Hohenbrink et al., 2016). Moreover, Thomas et al. (2012) found that damping accounted
370 for a large share of variance in a set of hydrographs from a region of 30,000 km². Damping was also the most relevant driver
371 of spatial variance in a set of time series of groundwater head at about the same scale (Lischeid et al., 2021).

372 **4.3 Limitations**

373 Data gaps during the studied period occurred due to multiple technical and environmental factors. Data gaps in soil moisture
374 time series were caused by repeated temporary failure of the WSN. There was a failure of one sensor that was replaced and
375 one LoRa node was damaged by intruding water. More relevant, however, were failures of data transmission. Yildiz et al.
376 (2015) point to the problem of optimizing transmission power for data and acknowledgement packets depending on energy
377 dissipation under the given conditions. E.g., saturated soil conditions and dense biomass stands reduce the transmission signal
378 from the node to the gateway (Bogena et al., 2009). The installation of a second gateway in September 2021 increased higher
379 transmission coverage in the field. Another obstacle was snow cover on the gateways' solar panels. Finally, solar panels were
380 subject to theft. However, higher level of maintenance and supervision helped to reduce the number and the length of data
381 gaps.

382 PCA requires gapless time series. Gaps in single time series need to be either filled at the risk of introducing artefacts or the
383 respective time period cannot be considered at all for analysis. This can be seen as a weakness of PCA. On the other hand, and
384 in contrast to other time series analysis approaches, the time series need not to be equidistant. Assigning PCs to processes and
385 effects is not straightforward and might be subject for debate. For example, in this study soil samples were taken at least at 0.8
386 m distance from the sensors to avoid disturbance of the measurements. Due to pronounced small-scale soil variability these
387 samples are not fully representative for the measurement sites. In spite of these limitations, the PCA results clearly point to
388 various effects worth to be studied in more detail in subsequent studies.

389 **5 Conclusion**

390 The use of PCA has a high value for the application in environmental sciences, as it contributes to process understanding of
391 soil water dynamics by disentangling the different effects of complex spatially and temporally diversified cropping systems.
392 In this study, more than 97% of the observed spatial and temporal variance was assigned to five different effects.
393 Meteorological drivers explained 72.3% of the total variance (PC1). Different seasonal patterns of root water uptake of winter
394 crops compared to summer crops accounted for another 17.0% of variance (PC2). An additional share of 2.2% of variance
395 seemed to be related to the effects of different vegetation cover and its interplay with soil hydraulic properties (PC4).
396 Heterogeneity of subsoil substrates explained 4.1 % of variance (PC3), and the damping effect of input signals over depth
397 another 1.7% (PC5). To summarize, plant-related direct and indirect effects accounted for 19.2% of the variance (PC2 and
398 PC4), and soil-related effects only for 5.8% (PC3 and PC5). In particular, the plant-induced effects on soil hydraulic properties
399 would be worthwhile to be studied in more detail.

400 Findings of this study highly depend on local conditions. However, the methodology itself is generally applicable to other site
401 conditions and can lead to improved management practices through improved knowledge about soil water dynamics.
402 Furthermore, information from this study can also help to develop both parsimonious and tailored mechanistic models for
403 model upscaling. In this regard, principal component analysis of large soil moisture data sets from real-world monitoring setups
404 performed a meaningful diagnostic tool for complex cropping systems.

405 **Acknowledgments**

406 The maintenance of the patchCROP experimental infrastructure and the LoRaWAN soil sensor system is ensured by the
407 Leibniz Centre for Agricultural Landscape Research. The authors acknowledge the additional support from the German
408 Research Foundation under Germany's Excellence Strategy, EXC-2070 – 390732324 – PhenoRob for patchCROP related
409 research activities.

410 The authors thank Gerhard Kast, Thomas von Oepen, Lars Richter, Robert Zieciak, Sigrid Ehlert and Motaz Abdelaziz for
411 their dedicated support in maintenance of the monitoring system and data collection.

412 **Competing interests**

413 The authors declare that they have no conflict of interest.

414 **References**

415 Acclima Inc.: True TDR310H. Soil-Water-Temperature-BEC-Sensor, 2019.

416 Acharya, B. S., Dodla, S., Gaston, L. A., Darapuneni, M., Wang, J. J., Sepat, S., and Bohara, H.: Winter cover crops effect on
417 soil moisture and soybean growth and yield under different tillage systems, *Soil and Tillage Research*, 195,
418 <https://doi.org/10.1016/j.still.2019.104430>, 2019.

419 Alhameid, A., Singh, J., Sekaran, U., Ozlu, E., Kumar, S., and Singh, S.: Crop rotational diversity impacts soil physical and
420 hydrological properties under long-term no- and conventional-till soils, *Soil Res.*, 58, 84, <https://doi.org/10.1071/SR18192>,
421 2020.

422 Baroni, G., Ortuani, B., Facchi, A., and Gandolfi, C.: The role of vegetation and soil properties on the spatio-temporal
423 variability of the surface soil moisture in a maize-cropped field, *Journal of Hydrology*, 489, 148–159,
424 <https://doi.org/10.1016/j.jhydrol.2013.03.007>, 2013.

425 BIRTHAL, P. S. and HAZRANA, J.: Crop diversification and resilience of agriculture to climatic shocks: Evidence from India,
426 *Agricultural Systems*, 173, 345–354, <https://doi.org/10.1016/j.agsy.2019.03.005>, 2019.

427 Bogena, H. R., Huisman, J. A., Meier, H., and Weuthen, A.: Hybrid wireless underground sensor networks: Quantification of
428 signal attenuation in soil, *Vadose Zone J.*, 8, 755-761, <https://doi.org/10.2136/vzj2008.0138>, 2009.

429 Bogena, H. R., Weuthen, A., and Huisman, J. H.: Recent Developments in Wireless Soil Moisture Sensing to Support Scientific
430 Research and Agricultural Management, *Sensors*, 22, 9792, <https://doi.org/10.3390/s22249792>, 2022.

431 Bönecke, E., Meyer, S., Vogel, S., Schröter, I., Gebbers, R., Kling, C., Kramer, E., Lück, K., Nagel, A., Philipp, G., Gerlach,
432 F., Palme, S., Scheibe, D., Zieger, K., Rühlmann, J.: Guidelines for precise lime management based on high-resolution soil
433 pH, texture and SOM maps generated from proximal soil sensing data, *Precision Agric*, 22, 493-523,
434 <https://doi.org/10.1007/s11119-020-09766-8>, 2021.

435 Bretherton, C. S., Smith, C., and Wallace, J. M.: An intercomparison of methods for finding coupled patterns in climate data,
436 *Journal of Climatology*, 5, 541–560, 1992.

- 437 Brocca, L., Melone, F., Moramarco, T., and Morbidelli, R.: Spatial-temporal variability of soil moisture and its estimation
438 across scales, *Water Resour. Res.*, 46, <https://doi.org/10.1029/2009WR008016>, 2010.
- 439 Brown, M., Heinse, R., Johnson-Maynard, J., and Huggins, D.: Time-lapse mapping of crop and tillage interactions with soil
440 water using electromagnetic induction, *Vadose zone j.*, 20, <https://doi.org/10.1002/vzj2.20097>, 2021.
- 441 Cardell-Oliver, R., Hübner, C., Leopold, M., and Beringer, J.: Dataset: LoRa Underground Farm Sensor Network, in:
442 Proceedings of the 2nd Workshop on Data Acquisition To Analysis - DATA'19, the 2nd Workshop, New York, NY, USA,
443 26–28, <https://doi.org/10.1145/3359427.3361912>, 2019.
- 444 Choi, M., Jacobs, J. M., and Cosh, M. H.: Scaled spatial variability of soil moisture fields, *Geophys. Res. Lett.*, 34,
445 <https://dx.doi.org/10.1029/2006GL028247>, 2007.
- 446 Deumlich, D., Ellerbrock, R. H., and Frielinghaus, Mo.: Estimating carbon stocks in young moraine soils affected by erosion,
447 *CATENA*, 162, 51–60, <https://doi.org/10.1016/j.catena.2017.11.016>, 2018.
- 448 Donat, M., Geistert, J., Grahmann, K., Bloch, R., and Bellingrath-Kimura, S. D.: Patch cropping- a new methodological
449 approach to determine new field arrangements that increase the multifunctionality of agricultural landscapes, *Computers and*
450 *Electronics in Agriculture*, 197, 106894, <https://doi.org/10.1016/j.compag.2022.106894>, 2022.
- 451 DIN ISO 11277: Soil quality - Determination of particle size distribution in mineral soil material - Method by sieving and
452 sedimentation (ISO 11277:1998 + ISO 11277:1998 Corrigendum 1:2002), Beuth-Verlag, Berlin,
453 <https://dx.doi.org/10.31030/9283499>, 2002.
- 454 DWD Climate Data Center (CDC): Historische tägliche Stationsbeobachtungen (Temperatur, Druck, Niederschlag,
455 Sonnenscheindauer, etc.) für Deutschland, Version v21.3, 2021.
- 456 Fischer, C., Roscher, C., Jensen, B., Eisenhauer, N., Baade, J., Attinger, S., Scheu, S., Weisser, W. W., Schumacher, J.,
457 Hildebrandt, A.: How Do Earthworms, Soil Texture and Plant Composition Affect Infiltration along an Experimental Plant
458 Diversity Gradient in Grassland?, *PLoS ONE*, 9, 6, <https://doi.org/10.1371/journal.pone.0098987>, 2014.
- 459 Fischer, G. F., Nachtergaele, S., Prieler, S., van Velthuizen, H. T., Verelst, L., and Wisberg, D.: Global Agro-ecological Zones
460 Assessment for Agriculture (GAEZ 2008), IIASA, Laxenburg, Austria and FAO, Rome, 2008.
- 461 GeoBasis-DE and Landesvermessung und Geobasisinformation Brandenburg (LGB): Digitales Geländemodell (DGM),
462 Landesvermessung und Geobasisinformation Brandenburg (LGB), Potsdam, 2021.
- 463 Graf, A., Bogena, H. R., Drüe, C., Herdelauf, H., Pütz, T., Heinemann, G., and Vereecken, H.: Spatiotemporal relations
464 between water budget components and soil water content in a forested tributary catchment, *Water Resour. Res.*, 50, 4837-
465 4857, <https://doi.org/10.1002/2013WR014516>, 2014.
- 466 Grahmann, K., Reckling, M., Hernandez-Ochoa, I., and Ewert, F.: An agricultural diversification trial by patchy field
467 arrangements at the landscape level: The landscape living lab “patchCROP,” in: Aspects of Applied Biology, Intercropping
468 for sustainability: Research developments and their application, 385–391, 2021.
- 469 Hohenbrink, T. L. and Lischeid, G.: Does textural heterogeneity matter? Quantifying transformation of hydrological signals
470 in soils, *Journal of Hydrology*, 523, 725–738, <https://doi.org/10.1016/j.jhydrol.2015.02.009>, 2015.
- 471 Hohenbrink, T. L., Lischeid, G., Schindler, U., and Hufnagel, J.: Disentangling the Effects of Land Management and Soil
472 Heterogeneity on Soil Moisture Dynamics, *Vadose Zone Journal*, 15, <https://doi.org/10.2136/vzj2015.07.0107>, 2016.

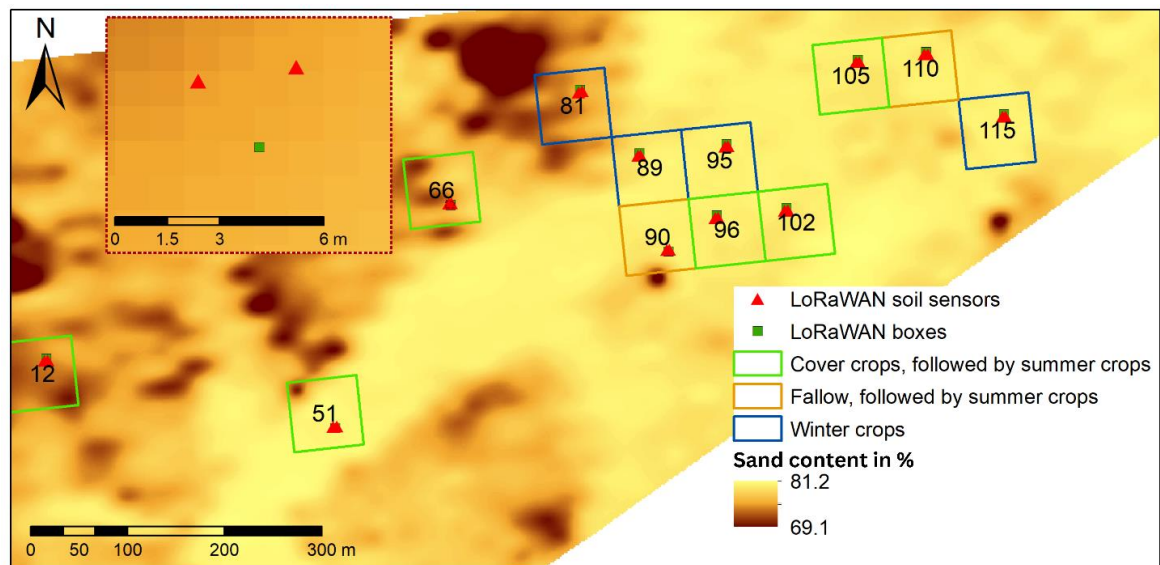
- 473 Hupet, F. and Vanclooster, M.: Intraseasonal dynamics of soil moisture variability within a small agricultural maize cropped
474 field, *Journal of Hydrology*, 261, 86–101, 2002.
- 475 IUSS Working Group WRB: World Reference Base for Soil Resources 2014, Update 2015, International Soil Classification
476 System for Naming Soils and Creating Legends for Soil Maps, World Soil Resources Reports No. 106, Rome: FAO, 2015.
- 477 Jolliffe, I. T.: Principal component analysis. Springer Series in Statistics, Springer, New York, 2002.
- 478 Joshi, C. and Mohanty, B. P.: Physical controls of near-surface soil moisture across varying spatial scales in an agricultural
479 landscape during SMEX02: Physical controls of soil moisture, *Water Resour. Res.*, 46,
480 <https://doi.org/10.1029/2010WR009152>, 2010.
- 481 Kaiser, H. F.: The Application of Electronic Computers to Factor Analysis, *Educ. Psychol. Measur.*, 20,
482 <https://doi.org/10.1177/001316446002000116>, 1960.
- 483 Karlen, D. L., Hurley, E. G., Andrews, S. S., Cambardella, C. A., Meek, D. W., Duffy, M. D., and Mallarino, A. P.: Crop
484 Rotation Effects on Soil Quality at Three Northern Corn/Soybean Belt Locations, *Agron.j.*, 98, 484–495,
485 <https://doi.org/10.2134/agronj2005.0098>, 2006.
- 486 Khan, H., Farooque, A. A., Acharya, B., Abbas, F., Esau, T. J., and Zaman, Q. U.: Delineation of Management Zones for Site-
487 Specific Information about Soil Fertility Characteristics through Proximal Sensing of Potato Fields, *Agronomy*, 10, 1854,
488 <https://doi.org/10.3390/agronomy10121854>, 2020.
- 489 Korres, W., Koyama, C. N., Fiener, P., and Schneider, K.: Analysis of surface soil moisture patterns in agricultural landscapes
490 using Empirical Orthogonal Functions, *Hydrol. Earth Syst. Sci.*, 14, 751–764, <https://doi.org/10.5194/hess-14-751-2010>, 2010.
- 491 Korres, W., Reichenau, T. G., Fiener, P., Koyama, C. N., Bogen, H. R., Cornelissen, T., Baatz, R., Herbst, M., Diekkrüger,
492 B., Vereecken, H., and Schneider, K.: Spatio-temporal soil moisture patterns – A meta-analysis using plot to catchment scale
493 data, *Journal of Hydrology*, 520, 326–341, <https://doi.org/10.1016/j.jhydrol.2014.11.042>, 2015.
- 494 Koudahe, K., Allen, S. C., Djaman, K.: Critical review of the impact of cover crops on soil properties, *International Soil and*
495 *Water Conservation Research*, 10, 343–354, <https://doi.org/10.1016/j.iswcr.2022.03.003>, 2022.
- 496 Krauss, L., Hauck, C., and Kottmeier, C.: Spatio-temporal soil moisture variability in Southwest Germany observed with a
497 new monitoring network within the COPS domain, *metz*, 19, 523–537, <https://doi.org/10.1127/0941-2948/2010/0486>, 2010.
- 498 Lange, B., Germann, P. F., and Lüscher, P.: Greater abundance of *Fagus sylvatica* in coniferous flood protection forests due
499 to climate change: impact of modified root densities on infiltration, *Eur J Forest Res*, 132, 151–163,
500 <https://doi.org/10.1007/s10342-012-0664-z>, 2013.
- 501 Lehr, C. and Lischeid, G.: Efficient screening of groundwater head monitoring data for anthropogenic effects and measurement
502 errors, *Hydrol. Earth Syst. Sci.*, 24, 501–513, <https://doi.org/10.5194/hess-24-501-2020>, 2020.
- 503 Lischeid, G., Frei, S., Huwe, B., Bogner, C., Lüers, J., Babel, W., and Foken, T.: Catchment Evapotranspiration and Runoff,
504 in: *Energy and Matter Fluxes of a Spruce Forest Ecosystem*, vol. 229, Springer, Cham, Cham, 355–375, 2017.
- 505 Lischeid, G., Dannowski, R., Kaiser, K., Nützmann, G., Steidl, J., and Stüve, P.: Inconsistent hydrological trends do not
506 necessarily imply spatially heterogeneous drivers, *Journal of Hydrology*, 596, 126096,
507 <https://doi.org/10.1016/j.jhydrol.2021.126096>, 2021.
- 508 Lloret, J., Sendra, S., Garcia, L., and Jimenez, J. M.: A Wireless Sensor Network Deployment for Soil Moisture Monitoring
509 in Precision Agriculture, *Sensors*, 21, 7243, <https://doi.org/10.3390/s21217243>, 2021.

- 510 Lueck, E. and Ruehlmann, J.: Resistivity mapping with Geophilus Electricus - Information about lateral and vertical soil
511 heterogeneity, *Geoderma*, 199, 2–11, <https://doi.org/10.1016/j.geoderma.2012.11.009>, 2013.
- 512 Mahmood, R., Littell, A., Hubbard, K. G., and You, J.: Observed data-based assessment of relationships among soil moisture
513 at various depths, precipitation, and temperature, *Applied Geography*, 34, 255–264,
514 <https://doi.org/10.1016/j.apgeog.2011.11.009>, 2012.
- 515 Martini, E., Wollschläger, U., Musolff, A., Werban, U., and Zacharias, S.: Principal Component Analysis of the Spatiotemporal
516 Pattern of Soil Moisture and Apparent Electrical Conductivity, *Vadose Zone J*, 16, vzj2016.12.0129,
517 <https://doi.org/10.2136/vzj2016.12.0129>, 2017.
- 518 Nied, M., Hundecha, Y., and Merz, B.: Flood-initiating catchment conditions: a spatio-temporal analysis of large-scale soil
519 moisture patterns in the Elbe River basin, *Hydrol. Earth Syst. Sci.*, 17, 1401–1414, <https://doi.org/10.5194/hess-17-1401-2013>,
520 2013.
- 521 Nunes, M. R., van Es, H. M., Schindelbeck, R., Ristow, A. J., Ryan, M.: No-till and cropping system diversification improve
522 soil health and crop yield, *Geoderma*, 328, 30-43, <https://doi.org/10.1016/j.geoderma.2018.04.031>, 2018.
- 523 Pan, F. and Peters-Lidard, C. D.: On the Relationship Between Mean and Variance of Soil Moisture Fields, *JAWRA Journal*
524 *of the American Water Resources Association*, 44, 235–242, <https://doi.org/10.1111/j.1752-1688.2007.00150.x>, 2008.
- 525 Paroda, Raj. S., Suleimenov, M., Yusupov, H., Kireyev, A., Medeubayev, R., Martynova, L., and Yusupov, K.: Crop
526 Diversification for Dryland Agriculture in Central Asia, in: *CSSA Special Publications*, edited by: Rao, S. C. and Ryan, J.,
527 *Crop Science Society of America and American Society of Agronomy*, Madison, WI, USA, 139–150,
528 <https://doi.org/10.2135/cssaspecpub32.c9>, 2015.
- 529 Placidi, P., Morbidelli, R., Fortunati, D., Papini, N., Gobbi, F., and Scorzoni, A.: Monitoring Soil and Ambient Parameters in
530 the IoT Precision Agriculture Scenario: An Original Modeling Approach Dedicated to Low-Cost Soil Water Content Sensors,
531 *Sensors*, 21, 5110, <https://doi.org/10.3390/s21115110>, 2021.
- 532 Prakosa, S. W., Faisal, M., Adhitya, Y., Leu, J.-S., Köppen, M., and Avian, C.: Design and Implementation of LoRa Based
533 IoT Scheme for Indonesian Rural Area, *Electronics*, 10, 77, <https://doi.org/10.3390/electronics10010077>, 2021.
- 534 R Development Core Team: R: A Language and Environment for Statistical Computing, R Foundation for Statistical
535 Computing (Version 4.1.0, <http://www.R-project.org>), Vienna, 2021.
- 536 Rodriguez, C., Mårtensson, L.-M. D., Jensen, E. S., and Carlsson, G.: Combining crop diversification practices can benefit
537 cereal production in temperate climates, *Agron. Sustain. Dev.*, 41, 48, <https://doi.org/10.1007/s13593-021-00703-1>, 2021.
- 538 Rossini, P. R., Ciampitti, I. A., Hefley, T., and Patrignani, A.: A soil moisture-based framework for guiding the number and
539 location of soil moisture sensors in agricultural fields, *Vadose zone J.*, 20, <https://doi.org/10.1002/vzj2.20159>, 2021.
- 540 Salam, A.: *Internet of Things for Sustainable Community Development: Wireless Communications, Sensing, and Systems*,
541 Springer International Publishing, Cham, Switzerland, <https://doi.org/10.1007/978-3-030-35291-2>, 2020.
- 542 Salam, A. and Raza, U.: *Signals in the Soil: Developments in Internet of Underground Things*, Springer International
543 Publishing, Cham, Switzerland, <https://doi.org/10.1007/978-3-030-50861-6>, 2020.
- 544 Scheffer, F. and Schachtschabel, P.: *Lehrbuch der Bodenkunde*, 15th ed., Spektrum Akademischer Verlag GmbH. Berlin,
545 Heidelberg, <https://doi.org/10.1007/978-3-662-55871-3>, 2002.

- 546 Scholl, P., Leitner, D., Kammerer, G., Loiskandl, W., Kaul, H.-P., and Bodner, G.: Root induced changes of effective 1D
547 hydraulic properties in a soil column, *Plant Soil*, 381, 193–213, <https://doi.org/10.1007/s11104-014-2121-x>, 2014.
- 548 Selzer, T., and Schubert, S.: Water dynamics of cover crops: No evidence for relevant water input through occult precipitation,
549 *J Agro Crop Sci.*, 209, 422-437, <https://doi.org/10.1111/jac.12631>, 2023.
- 550 Si, B. C.: Spatial Scaling Analyses of Soil Physical Properties: A Review of Spectral and Wavelet Methods, *Vadose Zone*
551 *Journal*, 7, 547–562, <https://doi.org/10.2136/vzj2007.0040>, 2008.
- 552 Sponagel, H., Grotenthaler, W., Hartmann, K.J., Hartwich, R., Janetzko, P., Joisten, H., Kühn, D., Sabel, K.J., Traidl, R.
553 (Eds.): *Bodenkundliche Kartieranleitung (German Manual of Soil Mapping, KA5)*, 5th edition, Bundesanstalt für
554 Geowissenschaften und Rohstoffe, Hannover, 2005.
- 555 Strebelle, S., Payrazyan, K., and Caers, J.: Modeling of a Deepwater Turbidite Reservoir Conditional to Seismic Data Using
556 Principal Component Analysis and Multiple-Point Geostatistics, *SPE Journal*, 8, 227–235, <https://doi.org/10.2118/85962-PA>,
557 2003.
- 558 Tamburini, G., Bommarco, R., Wanger, T. C., Kremen, C., van der Heijden, M. G. A., Liebman, M., and Hallin, S.:
559 Agricultural diversification promotes multiple ecosystem services without compromising yield, *Sci. Adv.*, 6, eaba1715,
560 <https://doi.org/10.1126/sciadv.aba1715>, 2020.
- 561 Taylor, J. and Whelan, B.: *A General Introduction to Precision Agriculture*, 2010.
- 562 Thomas, B., Lischeid, G., Steidl, J., and Dannowski, R.: Regional catchment classification with respect to low flow risk in a
563 Pleistocene landscape, *Journal of Hydrology*, 475, 392–402, <https://doi.org/10.1016/j.jhydrol.2012.10.020>, 2012.
- 564 Trnka, M., Rötter, R. P., Ruiz-Ramos, M., Kersebaum, K. C., Olesen, J. E., Žalud, Z., and Semenov, M. A.: Adverse weather
565 conditions for European wheat production will become more frequent with climate change, *Nature Clim Change*, 4, 637–643,
566 <https://doi.org/10.1038/nclimate2242>, 2014.
- 567 Vachaud, G., Passerat De Silans, A., Balabanis, P., Vauclin, M.: Temporal Stability of Spatially Measured Soil Water
568 Probability Density Function, *Soil Science Society of America Journal*, 49, 822-828,
569 <https://doi.org/10.2136/sssaj1985.03615995004900040006x>, 1985.
- 570 Vanderlinden, K., Vereecken, H., Hardelauf, H., Herbst, M., Martínez, G., Cosh, M. H., Pachepsky, Y. A.: Temporal Stability
571 of Soil Water Contents: A Review of Data and Analyses, *Vadose Zone J.*, <https://doi.org/10.2136/vzj2011.0178>, 2012.
- 572 Vereecken, H., Huisman, J. A., Pachepsky, Y., Montzka, C., van der Kruk, J., Bogaen, H., Weihermüller, L., Herbst, M.,
573 Martínez, G., and Vanderborght, J.: On the spatio-temporal dynamics of soil moisture at the field scale, *Journal of Hydrology*,
574 516, 76–96, <https://doi.org/10.1016/j.jhydrol.2013.11.061>, 2014.
- 575 Yang, L., Chen, L., and Wei, W.: Effects of vegetation restoration on the spatial distribution of soil moisture at the hillslope
576 scale in semi-arid regions, *CATENA*, 124, 138–146, <https://doi.org/10.1016/j.catena.2014.09.014>, 2015.
- 577 Yildiz, H. U., Tavli, B., and Yanikomeroglu, H.: Transmission power control for link-level handshaking in wireless sensor
578 networks, *IEEE Sensors Journal*, 16, 2, 561-576. 2015.
- 579 Zhao, X., Li, F., Ai, Z., Li, J., and Gu, C.: Stable isotope evidences for identifying crop water uptake in a typical winter wheat–
580 summer maize rotation field in the North China Plain, *Science of The Total Environment*, 618, 121-131,
581 <https://doi.org/10.1016/j.scitotenv.2017.10.315>, 2018.

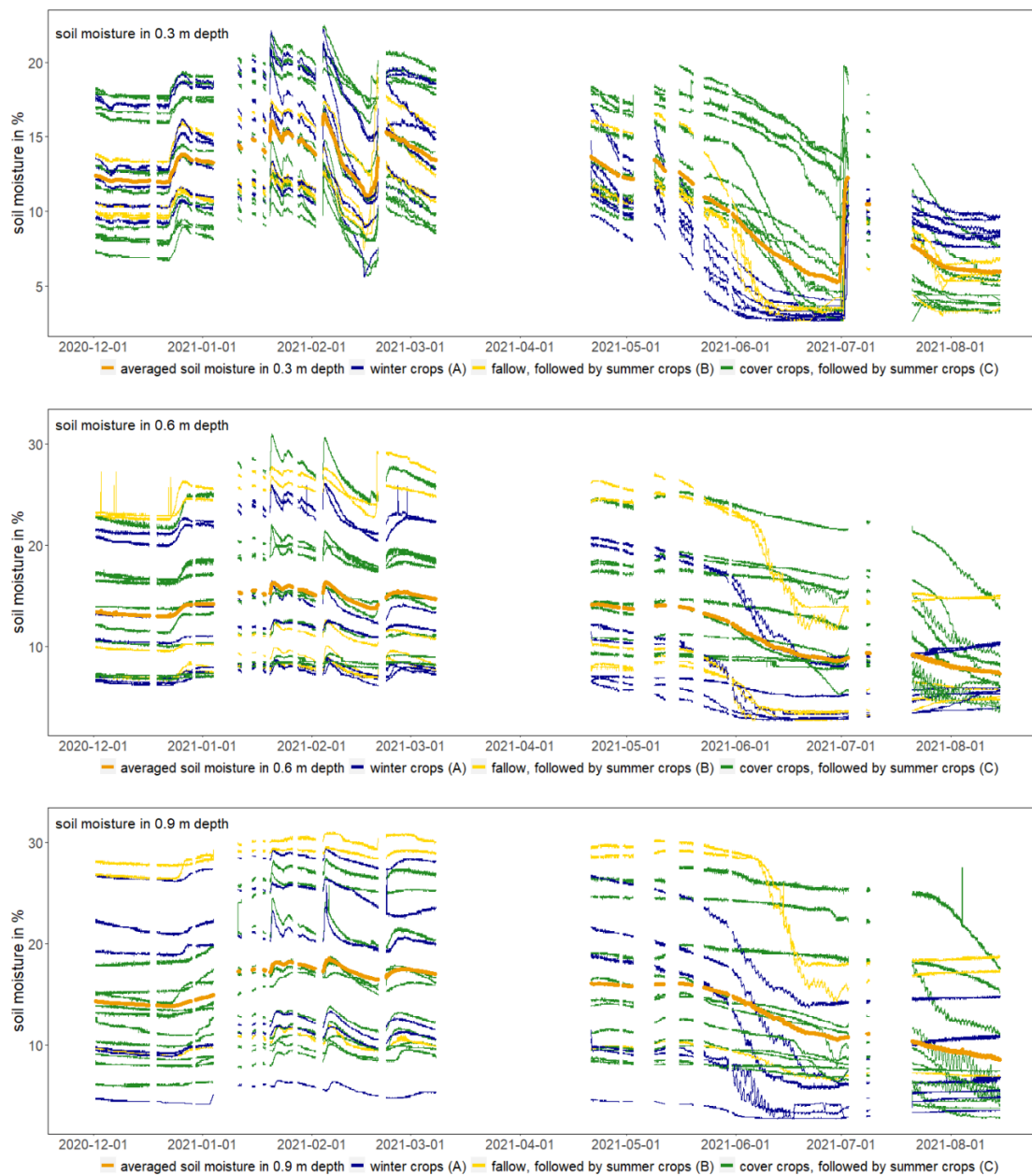
582 Zhao, Y., Peth, S., Wang, X. Y., Lin, H., and Horn, R.: Controls of surface soil moisture spatial patterns and their temporal
583 stability in a semi-arid steppe, *Hydrol. Process.*, 24, 2507–2519, <https://doi.org/10.1002/hyp.7665>, 2010.

584 **Figures and Tables**



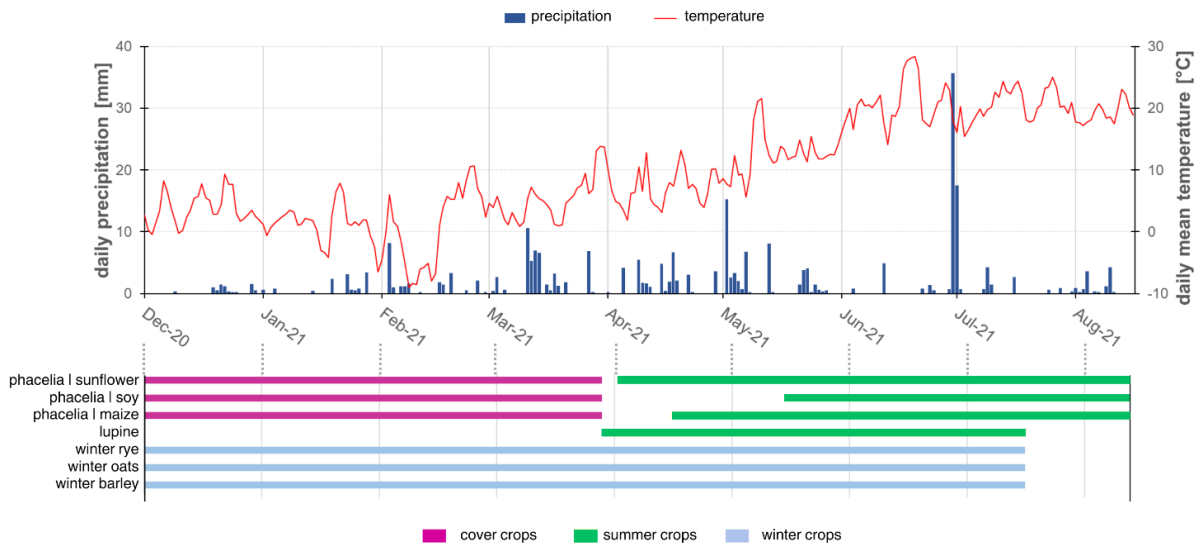
585

586 **Figure 1: Sand content in % in the top 0.25 m soil depth, location of the analysed patches, soil sensors (triangle) and boxes**
587 **(square) under different crop rotations at the patchCROP landscape laboratory, Tempelberg, Brandenburg, Germany.**



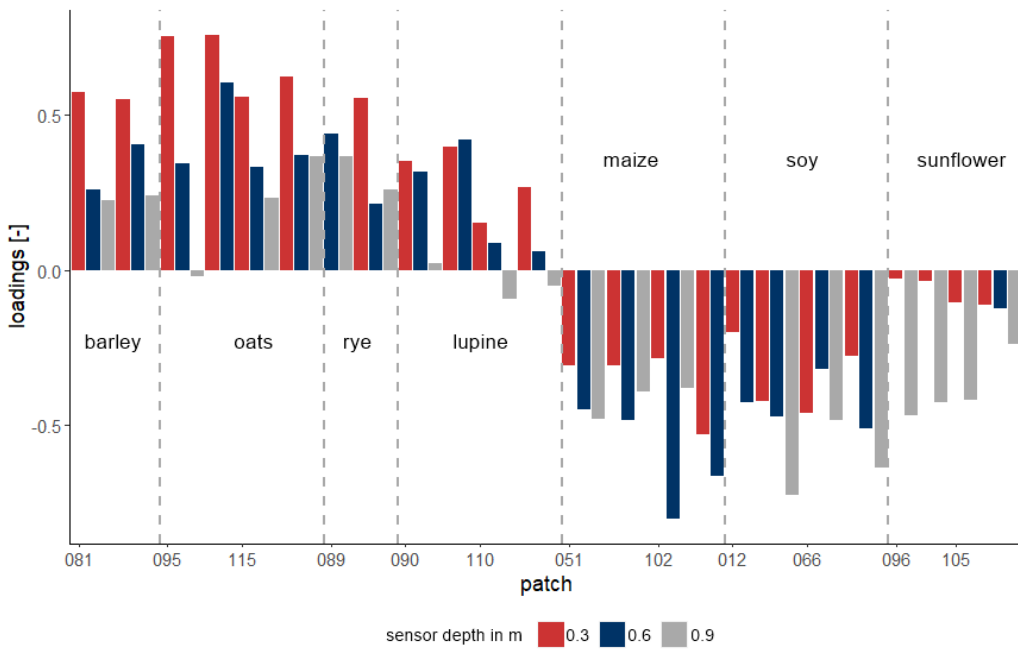
588

589 **Figure 2: Input soil moisture time series per depth, differentiated between crop groups, and average soil moisture of all time series**
 590 **per depth from 2020-12-01 until 2021-08-15 at the patchCROP landscape laboratory, Tempelberg, Brandenburg, Germany.**



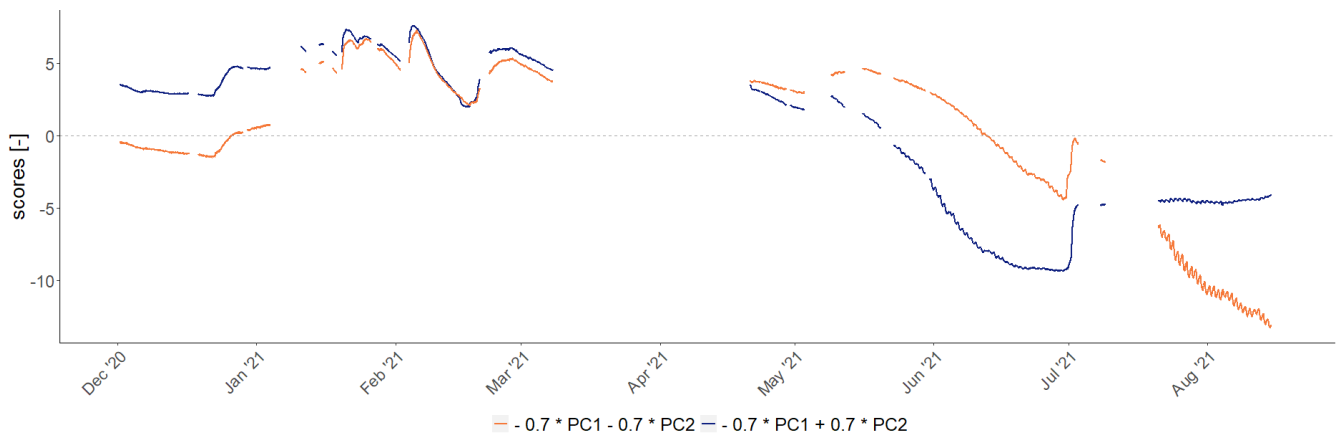
591

592 **Figure 3: Measured daily precipitation, mean temperature and cultivated crops - differentiated between winter crops (light blue**
 593 **bars), summer crops (green bars) and cover crops (pink bars) - from 2020-12-01 until 2021-08-15 at the patchCROP landscape**
 594 **laboratory, Tempelberg, Brandenburg, Germany. Specific crops for the studied timeframe stated at the left side of the horizontal**
 595 **bars.**



596

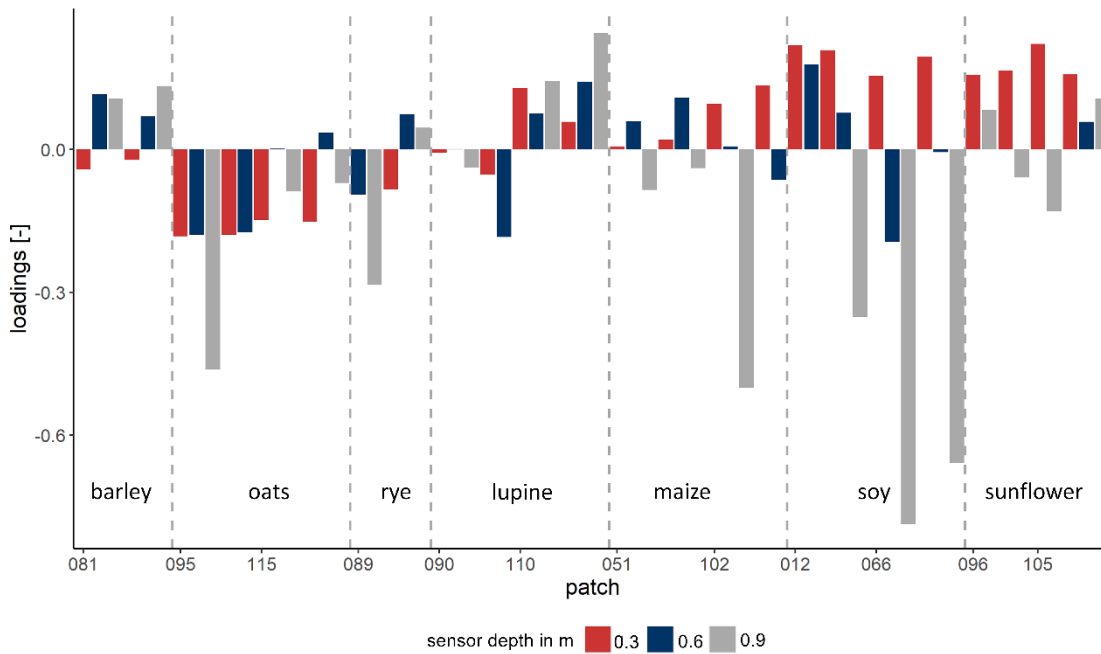
597 **Figure 4: Time series loadings on the second principal component at the patchCROP landscape laboratory, Tempelberg,**
 598 **Brandenburg, Germany, showing a crop group related pattern. Bars represent individual time series grouped by patch ID and**
 599 **sorted by crop.**



600

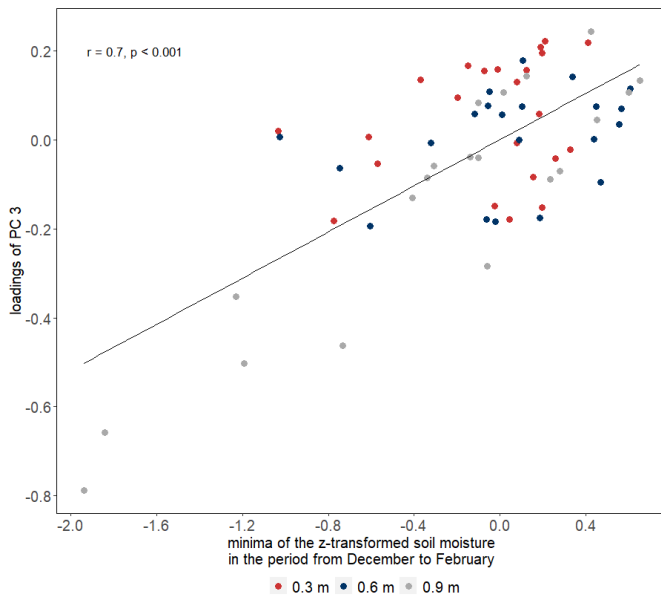
601 **Figure 5: Effect of the second principal component on modification of the general mean behaviour presented by the first principal**
 602 **component at the patchCROP landscape laboratory, Tempelberg. The blue line represents deviations from mean soil moisture for**
 603 **time series with positive loadings on PC2 (winter crops) while the orange line represents deviations from mean soil moisture for time**
 604 **series with negative loadings on PC2 (summer crops).**

605



606

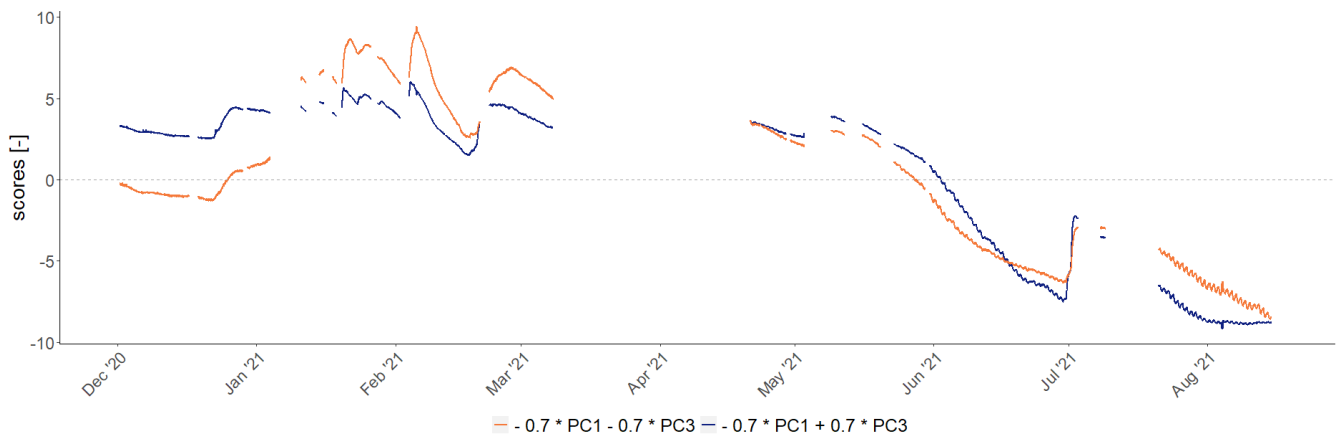
607 **Figure 6: Loadings of time series on the third principal component at the patchCROP landscape laboratory, Tempelberg,**
 608 **Brandenburg, Germany with some of the sensors in deeper layers showing noticeably negative loadings. Bars represent individual**
 609 **time series grouped by patch ID and sorted by crop.**



610

611 **Figure 7: Relation between minima of the z-transformed soil moisture in the first months of the study period with loadings of third**
 612 **principal component showing that sensors with noticeably negative loadings showed distinctly negative z-transformed minima.**

613



614

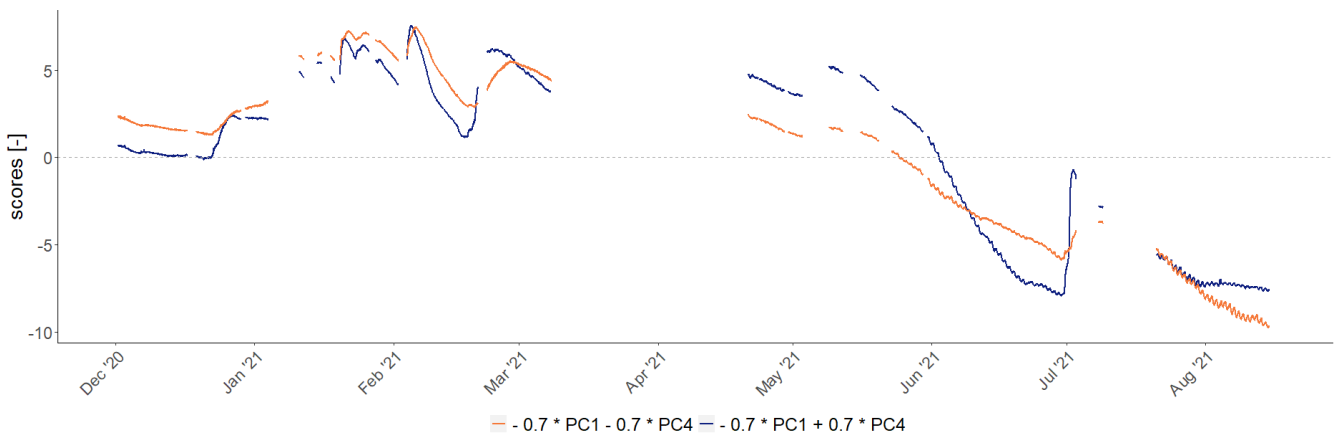
615 **Figure 8: Effect of the third principal component on modification of the general mean behaviour presented by the first principal**
 616 **component at the patchCROP landscape laboratory, Tempelberg. The blue line represents deviations from mean soil moisture for**
 617 **time series with positive loadings on PC3 (majority of the time series) while the orange line represents deviations from mean soil**
 618 **moisture for time series with negative loadings on PC3 (part of the sensors in 0.9 m depth).**



620

621 **Figure 9: Loadings of time series on the fourth principal component at the patchCROP landscape laboratory, Tempelberg,**
 622 **Brandenburg, Germany showing mainly negative loadings for crop group A, positive loadings for crop group B and loadings with**
 623 **no clear pattern for crop group C. Bars represent individual time series grouped by patch ID, sorted by treatment group.**

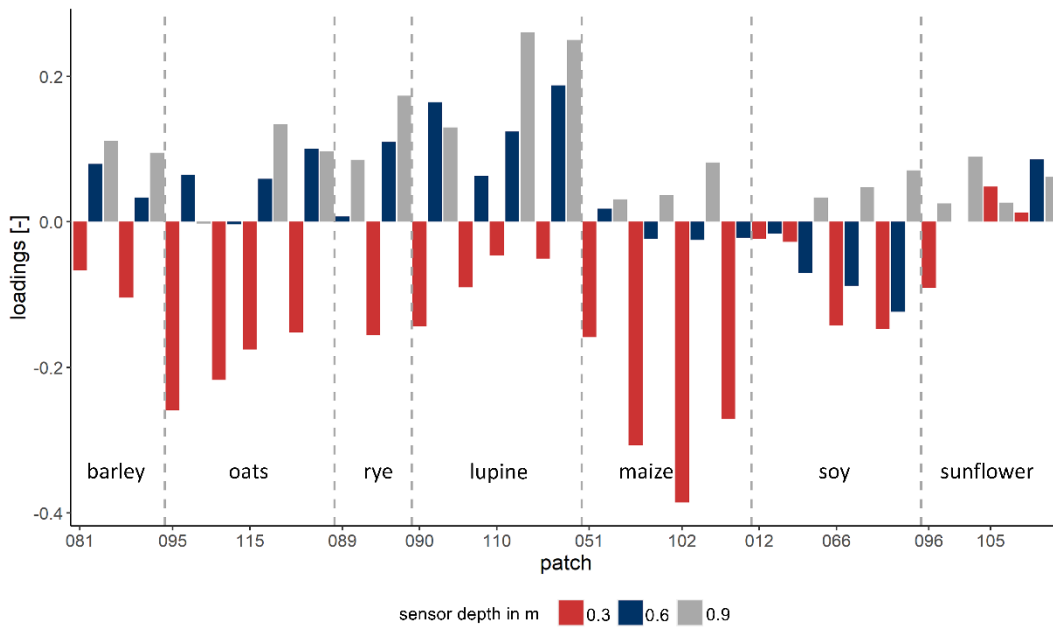
624



625

626 **Figure 10: Effect of the fourth principal component on modification of the general mean behaviour presented by the first principal**
 627 **component at the patchCROP landscape laboratory, Tempelberg. The blue line represents deviations from mean soil moisture for**
 628 **time series with positive loadings on PC4 (single sensors of crop group A, all sensors of crop group B, and part of crop group C)**
 629 **while the orange line represents deviations from mean soil moisture for time series with negative loadings on PC4 (most sensors of**
 630 **crop group A and part of the sensors of crop group C).**

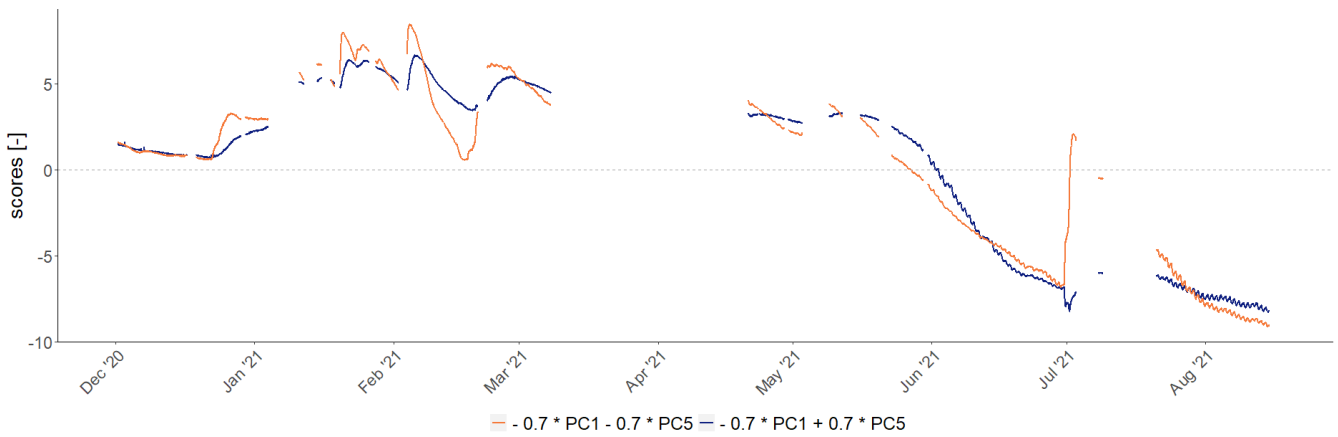
631



632

633 **Figure 11: Loadings of time series on the fifth principal component at the patchCROP landscape laboratory showing a depth**
 634 **related pattern. Bars represent individual time series grouped by patch ID, sorted by crop.**

635



636

637 **Figure 12: Effect of the fifth principal component on modification of the general mean behaviour presented by the first principal**
 638 **component at the patchCROP landscape laboratory, Tempelberg. The blue line represents deviations from mean soil moisture for**
 639 **time series with positive loadings on PC5 (sensors in greater depth) while the orange line represents deviations from mean soil**
 640 **moisture for time series with negative loadings on PC5 (sensors in shallow depth).**

641 **Table 1: Overview of crop rotation, sand content in the top 0.25 m soil depth and weed control for selected patches at the patchCROP**
 642 **landscape laboratory, Tempelberg, Brandenburg, Germany.**

Crop in winter season	Crop in summer season	Crop group	Sand content (in 1 m buffer zone around sensors) in %	Weed control	Patch ID
Winter barley		A	78.3	conventional	81
Winter oats		A	80.7	conventional	95
Winter oats		A	80.6	reduced	115
Winter rye		A	80.5	conventional	89
Fallow	Lupine	B	80.6	conventional	90
Fallow	Lupine	B	80.3	reduced	110
Phacelia	Maize	C	80.8	reduced	51
Phacelia	Maize	C	80.6	conventional	102
Phacelia	Soy	C	78.5	reduced	12
Phacelia	Soy	C	77.9	conventional	66
Phacelia	Sunflower	C	80.6	conventional	96
Phacelia	Sunflower	C	80.5	reduced	105

643

644 **Table 2: Overview of normalized difference vegetation index (NDVI), surface temperature, and slope at the locations of analysed**
 645 **sensors at the patchCROP experiment in Tempelberg, Brandenburg, Germany.**

Crop	Patch ID	Sensor Position	NDVI 2021-05-20 [-]	NDVI 2021-05-31 [-]	NDVI 2021-07-06 [-]	Surface Temperature 2021-05-31 in °C	Slope in °
Winter barley	81	West	0.874	0.182	0.926	20.57	2.01
Winter barley	81	East	0.875	0.180	0.927	20.43	1.94
Winter oats	95	East	0.838	0.208	0.834	27.25	1.36
Winter oats	95	West	0.838	0.213	0.840	27.85	1.15
Winter oats	115	West	0.756	0.278	0.845	23.70	1.28
Winter oats	115	East	0.783	0.281	0.863	25.12	0.43
Winter rye	89	West	0.796	0.263	0.856	22.39	1.74
Winter rye	89	East	0.787	0.206	0.822	24.95	1.67
Lupine	90	West	0.185	0.395	0.710	26.31	1.40
Lupine	90	East	0.203	0.391	0.733	24.96	1.27
Lupine	110	West	0.090	0.563	0.635	26.98	1.88
Lupine	110	East	0.090	0.567	0.639	26.76	2.50

Maize	51	West	-0.099	0.654	0.181	35.44	0.82
Maize	51	East	-0.096	0.638	0.217	35.29	0.93
Maize	102	West	-0.077	0.714	0.175	37.88	0.88
Maize	102	East	-0.058	0.728	0.178	38.03	0.90
Soy	12	West	-0.107	0.748	0.166	34.87	1.71
Soy	12	East	-0.108	0.723	0.162	34.44	1.11
Soy	66	West	-0.115	0.730	0.144	35.09	2.40
Soy	66	East	-0.114	0.661	0.147	34.39	2.13
Sunflower	96	West	-0.109	0.816	0.211	33.76	0.59
Sunflower	96	East	-0.101	0.827	0.229	34.70	0.69
Sunflower	105	West	0.178	0.610	0.564	29.79	1.04
Sunflower	105	East	0.030	0.696	0.399	34.53	1.00

646

647 **Table 3: Statistical characteristics and interpretations of principal components 1 to 5 for soil moisture dynamics of selected patches**
648 **at the patchCROP landscape laboratory, Tempelberg, Brandenburg, Germany.**

	PC1	PC2	PC3	PC4	PC5
Eigenvalue	46.25	10.89	2.60	1.43	1.06
Proportion of variance in %	72.27	17.01	4.06	2.23	1.65
Proportion of variance (cumulative) in %	72.27	89.28	93.34	95.57	97.22
Interpretation	Mean behaviour	Winter vs. summer crops	Subsoil texture	winter vegetation cover and influence of cover crops on soil	Damping of the input signal
Prevailing driver	weather	crop	soil	crop and soil	soil

649

650 **Table 4: Pearson correlation coefficients between surface temperature and normalized difference vegetation index (NDVI) at the**
651 **patchCROP landscape laboratory, Tempelberg, Brandenburg, Germany, and loadings of sensors in all depths or at single depths,**
652 **respectively, on the second principal component. All correlations were highly significant ($p < 0.01$).**

Variable	Sensors in all depths	0.3 m	0.6 m	0.9 m
Surface temperature	-0.853	-0.881	-0.909	-0.916
NDVI 2021-05-20	0.836	0.904	0.837	0.907
NDVI 2021-05-31	0.899	0.945	0.944	0.946

NDVI 2021-07-06

-0.860

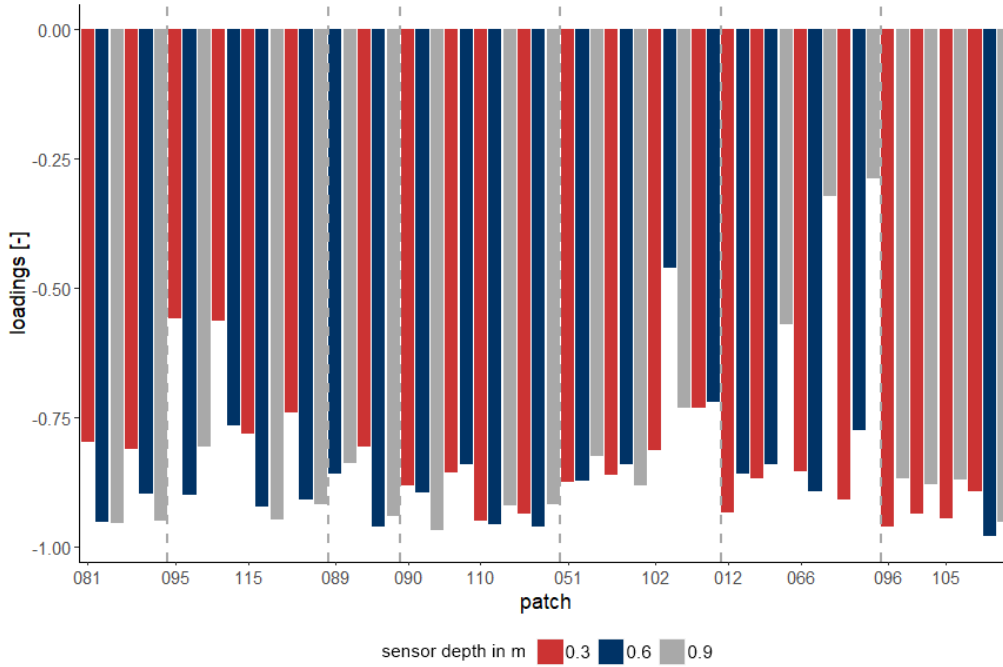
-0.898

-0.917

-0.913

653

654 APPENDIX A



655

656 Figure 13: Loadings of time series on the first principal component at the patchCROP landscape laboratory, Tempelberg,
657 Brandenburg, Germany. Bars represent individual time series grouped by patch ID and sorted by crop.